Connectivity of confined 3D Networks with Anisotropically Radiating Nodes

Orestis Georgiou[1,2], Carl P. Dettmann[2], and Justin P. Coon[3]

[1]Toshiba Telecommunications Research Laboratory, 32 Queens Square, Bristol, BS1 4ND, UK
[2]School of Mathematics, University of Bristol, University Walk, Bristol, BS8 1TW, UK
[3]Department of Engineering Science, University of Oxford, Parks Road, OX1 3PJ, Bristol, UK

***Abstract*—Nodes in ad hoc networks with randomly oriented directional antenna patterns typically have fewer short links and more long links which can bridge together otherwise isolated subnetworks. This network feature is known to improve overall connectivity in 2D random networks operating at low channel path loss. To this end, we advance recently established theoretical results to obtain analytic expressions for the mean degree of 3D networks for simple but practical anisotropic gain profiles, including those of patch, dipole and end-fire array antennas. Our analysis reveals that for homogeneous systems (i.e. neglecting boundary effects) directional radiation patterns are superior to the isotropic case only when the path loss exponent is less than the spatial dimension. Moreover, we establish that ad hoc networks utilizing directional transmit and isotropic receive antennas (or vice versa) are always sub-optimally connected regardless of the environment path loss. We extend our analysis to investigate inhomogeneous systems, and study the geometrical reasons why boundary effects cause directional radiating nodes to be at a disadvantage to isotropic ones. Finally, we discuss multi-directional gain patterns consisting of many equally spaced lobes which could be used to mitigate boundary effects and improve overall network connectivity.**

I. Introduction

Wireless ad hoc networks do not rely on any pre-existing infrastructure such as routers or access points and so can be deployed on the fly [1]. Equipped with multihop relaying and signal processing capabilities, they can self-organize and dynamically optimize network performance, traits which are becoming increasingly useful in sensor and vehicular network applications [2], including, *inter alia*, smart grid, exploration and environmental monitoring over extended 3D regions, disaster detection and/or search-and-rescue operations in hazardous/disaster relief areas, swarm robotics, road safety message dissemination, traffic management and dynamic route planning. Commonality in these applications can be found in that the number and distribution of nodes in the networks is often random, as was realized and studied by Gupta and Kumar in 1998 [3]. From a communications perspective, understanding the connectivity properties of random networks[1] has ever since been of paramount importance as it can lead to improved network design, protocols [7], [8] and deployment methodologies [9]–[11].

orestis.georgiou@toshiba-trel.com

[1]A plethora of relevant problems and solutions can be found in the mathematical literature under random graph theory [4], and in physics under percolation theory [5], [6].

It is often assumed, that when deployed, ad hoc networks will be well connected. To date, many works have challenged this assumption and have theoretically investigated a number of network features and variants. Most however adopt one or more of the following assumptions: the network resides in an extended two dimensional domain[2], nodes are isotropically radiating, links between nodes are formed deterministically according to a fixed range (i.e. hard-disk type connections), and/or the number of nodes $N \to \infty$. In what follows we will lift all of these assumptions.

We are interested in the effect of *randomized beamforming* strategies[3] which are known to improve network connectivity at low path loss exponents. How this improvement is achieved was first addressed in [13], and later in [14] where it was argued that randomized beamforming cannot be said to strictly improve/degrade connectivity. To this end, it was numerically estimated in [15] (and similar papers by the same authors) that the critical path loss exponent below which improvements are observed is 3. This was analytically pushed down to 2 in [16] for homogeneous domains where it was also shown that this number is independent of the small-scale fading model used. Finally, the possibility of using multi-directional antennas was proposed and studied in [17], and although unmotivated, was reported to enhance connectivity at low path loss. All the above works are restricted to two dimensional networks.

It is this partial understanding that motivates the current investigation where we consider finite and confined three dimensional networks with anisotropically radiating nodes, that connect in probability space using well established statistical fading models. To this end, we provide general analytic formulas for the connectivity mass[4] of several simple but practical radiation pattern approximations (including those of patch, dipole and end-fire array antennas) and conclusively show *when and how* randomized beamforming of anisotropically radiating nodes can improve or worsen the connectivity of ad hoc networks[5]. Namely, we find that in the absence of boundary effects, directional antennas yield superior perfor-

[2]Some works consider bounded domains but scale volume exponentially with the number of nodes, thus ignoring any boundary effects [12].

[3]In randomized beamforming, each anisotropically radiating node selects a boresight direction randomly and independently on the unit sphere.

[4]The connectivity mass (defined in (5)) is a measure of the connectivity properties of a node in the network and is related to several other network observables.

[5]In all cases, the gain is properly normalized as to ensure a fair comparison.

mance when the path loss exponent η is less than the spatial dimension d, and inferior when $\eta > d$. Moreover, when $\eta = d$, network connectivity is found to be invariant to the antenna gain details. This simple and attractive picture is however radically different in confined spaces. We show that in the presence of boundaries, the advantages of directional antennas are significantly undermined due to the existence of 'blind spots', which effectively decrease the network mean degree and increase the likelihood of node isolation. Therefore, we propose and investigate multi-directional radiation patterns as a means to mitigate boundary effects. We stress that while hardware functionality may vary in realistic networks deployed in for example so called smart buildings for sensing, tracking, or control purposes, our analysis captures the underlying network connectivity features on both local and global scales. This enables simple design recommendations to be extracted depending on the ratio d/η and the local network topology. Consequently, global network connectivity and functionality can be enhanced through many local considerations in a distributed fashion.

The paper is structured as follows: Sec. II introduces the system set-up and all relevant parameters and assumptions. Sec. III discusses various network observables and identifies the connectivity mass as a key quantity of interest. Sec. IV investigates the connectivity mass for homogeneous systems (i.e. ignoring boundary effects) and derives analytic expressions for simple but practical gain profiles which are then verified through extensive computer simulations which calculate both the mean degree and the probability of node isolation. Based on these expressions, the analysis presented in Sec. V reveals that the connectivity properties of ad hoc networks scale with the solid angle over which the gain is concentrated on. Sec. VI examines the effect of boundaries in inhomogeneous systems and identifies the weaknesses of directional patterns. Sec. VII proposes a multi-directional solution to mitigate boundary effects and investigates the optimal radiation pattern for a rectangular cuboid domain. Finally, Sec. VIII summarises and discusses our main results and highlights some ideas and challenges for future research.

II. Network Definitions and System Model

We begin our discussion by describing the system set-up and all relevant parameters and assumptions. We consider a network consisting of N identical nodes with locations $\mathbf{r}_i$ for $i = 1, \ldots, N$, chosen randomly inside a three dimensional domain $\mathcal{V} \subseteq \mathbb{R}^3$ of volume V. The density of nodes is assumed uniform and is given by $\rho = N/V$. The antenna orientations $\hat{\mathbf{v}}_i$ are also chosen at random from a uniform distribution supported on the surface area of the unit sphere S^2. Such node distributions are often used to model vehicular and ad hoc wireless networks [1], [2].

Assuming negligible inter-node interference, we define the connection probability between nodes i and j separated by a distance $r_{ij} = |\mathbf{r}_i - \mathbf{r}_j| \geq 0$ through the relation

$$H(r_{ij}) = P(\log_2(1 + \text{SNR} \cdot |h|^2) \geq \wp), \tag{1}$$

signifying that the channel between them can support a rate of at least $\wp$. It is worth noting that other definitions can be adopted for $H(r_{ij})$ such as the target bit-error probability or the complement of the information outage probability. For the sake of brevity we will henceforth write H_{ij} instead of $H(r_{ij})$ unless otherwise stated.

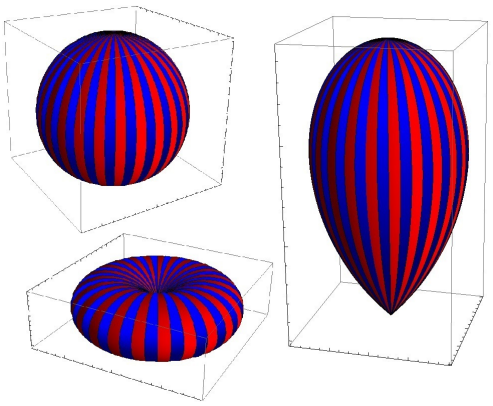

Fig. 1. Simplified gain patterns of a patch, dipole, and horn or end-fire array antennas.

In equation (1), SNR denotes the long-term average received signal-to-noise ratio and h is the channel transfer coefficient for single input single output (SISO) antenna systems. Without loss of generality, we assume lossless antennas with equal transmit and receive performances. We therefore have from the Friis transmission formula that

$$\text{SNR} \propto G_i G_j r_{ij}^{-\eta} \tag{2}$$

where η is the path loss exponent[6], G_i is the gain of the antenna at node i observed in the direction of node j and G_j is the gain of the antenna at node j observed in the direction of node i. The gain functions represent the ratio between the signal intensity in a given direction, and the signal intensity had the same power been radiated isotropically. In order to keep the mathematics tractable, we will ignore small sidelobes and backlobes (as done in many other studies) and mostly restrict our analysis to rotationally symmetric gain patterns (i.e. surfaces of revolution) about some orientation unit vector $\hat{\mathbf{v}}$. It follows that isotropic radiation patterns have a constant gain $G = 1$, while anisotropic ones are functions of the polar angle θ about $\hat{\mathbf{v}}$, appropriately normalized by the condition

$$\int_0^{2\pi} \int_0^{\pi} G(\theta) \sin\theta \mathrm{d}\theta \mathrm{d}\phi = 4\pi. \tag{3}$$

At a later stage, we will also consider *multi-directional* radiation patterns of the form

$$G(\theta, \phi) = \sum_{k=1}^{n} g_k(\theta^{(k)}), \tag{4}$$

where the g_k characterize the gain function for the k-th directional lobe, and $\theta^{(k)}$ is the angle measured from a collection of unit vectors $\Theta = \{\hat{\mathbf{v}}^{(k)}, \text{ for } k = 1, \ldots, n\}$. Note that multi-directional radiation patterns are typically not surfaces

[6]Typically $\eta = 2$ corresponds to propagation in free space but for cluttered environments it is observed to be $\eta > 2$. Values of $\eta < 2$ have been reported, typically for indoor environments, for example in grocery stores [18].

of revolution, but their individual components g_k are. We adjourn further development of this notation until the relevant subsections.

Complicated radiation patterns can be achieved using a variety of beamforming techniques [19]. In the simplest case this would involve a number of isotropic radiating antenna elements arranged in a linear, circular or planar array with variable transmit and receive powers and appropriately tuned phase shifts. If done correctly, the constructive/destructive electromagnetic interference results in the desired radiation pattern. Achieving perfect beamforming across large networks however is an idealized and relatively costly system requirement. Therefore, we adopt here a simpler strategy by choosing the antenna orientation vector $\hat{\mathbf{v}}$ of each node at random thus offering a simple and practical deployment method at low hardware complexity and minimal communication overhead.

In summary, our system model, as defined above, has three sources of randomness: random node positions, random antenna orientations, and random pair connection probabilities according to the channel fading model. In what follows, we investigate the connectivity properties at both the local vicinity of each node and the global network topology using simple but practical radiation patterns, characteristic of relatively cheap and readily available antennas, e.g., patch, dipole, and horn or end-fire arrays (see illustrations in Fig. 1). For the reader's convenience we include in Table I a list of the above defined parameters for future reference.

TABLE I
NOTATION AND SYMBOLS USED IN THE PAPER

Symbol	Definition / Explanation
η	Path loss exponent
N	Number of nodes
$\mathcal{V}$	Domain in which network nodes are deployed
$\mathbf{r}_i$	Vector describing the position of node i in $\mathcal{V}$
$\hat{\mathbf{v}}_i$	Vector describing the antenna orientation of node i
r_{ij}	Euclidean distance between nodes i and j
V	Domain volume
ρ	Density of nodes equal to N/V
G_i	Antenna gain of node i in the direction of node j
H_{ij}	Probability that the pair (i,j) is connected

III. NETWORK CONNECTIVITY AND CONNECTIVITY MASS

There exist a plethora of measures of the connectivity properties of a complex network [6]. These include for example clustering statistics, network modularity measures, the number of independent paths, algebraic connectivity, etc. Each of these measures offers different information and one must choose wisely which ones are useful to the intended application. Here, we restrict our attention to four closely related observables, namely we study 1) the pair formation probability p_2, 2) the degree distribution $d(k)$, 3) the minimum network degree $P_{md}(k)$, and 4) the probability that a random network with randomly oriented antennas is fully connected P_{fc}. In what follows, we will argue that all four observables can be effectively characterized through the *connectivity mass* $\mathsf{M}(\mathbf{r}_i, \hat{\mathbf{v}}_i)$, thus rendering it a key metric of interest, which we will study for both homogeneous and inhomogeneous domains in the subsequent sections. We define the connectivity mass of a node i through the relation

$$\mathsf{M}(\mathbf{r}_i, \hat{\mathbf{v}}_i) = \frac{1}{4\pi} \int\!\!\int_{\mathcal{V}} H_{ij} \mathrm{d}\mathbf{r}_j \mathrm{d}\Omega_j, \tag{5}$$

where $\mathrm{d}\Omega = \sin\vartheta \mathrm{d}\vartheta\mathrm{d}\varphi$ denotes the differential solid angle in spherical coordinates and the integration is performed over the unit sphere $S^2 = [0,\pi) \times [0, 2\pi)$. Note that we will use curly symbols (ϑ, φ) for orientation coordinates, and normal ones (θ, ϕ) for position coordinates.

A. Pair Formation Probability

The physical significance of the connectivity mass becomes apparent through the simple relation

$$H_i = \frac{\mathsf{M}(\mathbf{r}_i, \hat{\mathbf{v}}_i)}{V}, \tag{6}$$

describing the probability that node i situated at $\mathbf{r}_i$ connects with a randomly chosen node j. This probability is obtained by averaging over all possible node positions $\mathbf{r}_j \in \mathcal{V}$ and all possible antenna orientations Ω_j. Integrating (6) once more gives the probability that two randomly selected nodes connect to form a pair

$$p_2 = \frac{1}{4\pi V} \int\!\!\int_{\mathcal{V}} H_i \mathrm{d}\mathbf{r}_i \mathrm{d}\Omega_i. \tag{7}$$

B. Degree Distribution

Since node locations and orientations are independent, the probability that node i has degree k (i.e. connects with exactly k other nodes) is given by the binomial distribution

$$d_i(k) = \binom{N-1}{k} H_i^k (1-H_i)^{N-1-k}. \tag{8}$$

If N is large and H_i is small, (8) can be well approximated by the Poisson distribution

$$d_i(k) \approx \frac{\mu_i^k}{k!} e^{-\mu_i}, \qquad D_i(k) = \sum_{m=0}^{k} d_i(m), \tag{9}$$

where $\mu_i = (N-1)H_i$, and $D_i(k)$ is the corresponding cumulative distribution function. The Poisson approximation in (9) is justified if $V \gg 1$, thus making H_i small. Finally, to obtain the degree distribution we average over all possible node positions and all possible antenna orientations to obtain

$$d(k) = \frac{1}{4\pi V} \int\!\!\int_{\mathcal{V}} d_i(k) \mathrm{d}\mathbf{r}_i \mathrm{d}\Omega_i. \tag{10}$$

The average number of nodes connected to a typical node in the network is called the mean degree and is simply given by

$$\mu = \frac{1}{4\pi V} \int\!\!\int_{\mathcal{V}} \mu_i \mathrm{d}\mathbf{r}_i \mathrm{d}\Omega_i = (N-1)p_2. \tag{11}$$

C. Minimum network degree

From the degree distribution, it is straight forward to derive $P_{md}(k)$ defined as the probability that the network has minimum degree k. Assuming that for $N \gg 1$, the degree of node i is almost independent of the degree of node $j \neq i$ (this is true if i and j are not directly connected), it follows that [20]

$$P_{md}(k) = \prod_{i=1}^{N} P(\text{degree}(\mathbf{r}_i) \geq k) = \prod_{i=1}^{N} \left(1 - D_i(k-1)\right). \tag{12}$$

In a homogeneous system (i.e. when there are no boundary effects) the ith node's position and orientation is arbitrary. This implies that $d(k) = d_i(k)$ and $\mu = \mu_i \ \forall i$ such that

$$P_{md}(k) = \left[1 - \sum_{m=0}^{k-1} \frac{\mu^k}{k!} e^{-\mu}\right]^N = 1 - N \sum_{m=0}^{k-1} \frac{\mu^m}{m!} e^{-\mu} + \ldots \tag{13}$$

Note that if the mean degree μ is large enough, correction terms denoted in (13) as $(\ldots)$ will be exponentially smaller, and can thus be neglected to yield a concise approximation of P_{md}. For inhomogeneous systems the above picture is incomplete as boundary effects play an important role.

D. Full Connectivity

A network is said to be fully connected if any node can communicate with any other node in a multihop fashion. While a very strong measure of connectivity, P_{fc} is compatible with delay and/or disruption tolerant networking. This field was recently popularized by the Defence Advanced Research Projects Agency (DARPA) in an attempt to increase wireless network reliability and prevent disruptions due to: radio range, node sparsity, energy resources, attack, noise, etc. [21], [22].

1) Isotropic Case: For isotropic radiation ($G = 1$), a theory for P_{fc} was recently developed in [23] for arbitrary dimension $d \geq 2$ using an exact cluster expansion approach derived from statistical physics. The authors main result expressed P_{fc} at high densities as the complement of the probability of an isolated node

$$P_{fc} = 1 - \rho \int_{\mathcal{V}} e^{-\rho \int_{\mathcal{V}} H_{ij} \mathrm{d}\mathbf{r}_j} \mathrm{d}\mathbf{r}_i. \tag{14}$$

Clearly, if $\int_{\mathcal{V}} H_{ij} \mathrm{d}\mathbf{r}_j < \infty$ we have that $P_{fc} = 1$ in the limit of $\rho \to \infty$. As the density of nodes is decreased from ∞, the most likely way that a network becomes *not* fully connected is through an isolated node. This is exactly what (14) describes. As the density of nodes is decreased further, several nodes may become isolated and may even group together and form isolated pairs (see [23] for more details). At such densities or lower, equation (14) becomes obsolete and thus inaccurate[7].

2) Anisotropic Case: Equation (14) can be generalized for anisotropic radiation patterns and can account for the randomly oriented nodes in a straightforward way as follows

$$\begin{aligned} P_{fc} &= 1 - \frac{\rho}{4\pi} \iint_{\mathcal{V}} e^{-\frac{\rho}{4\pi} \iint_{\mathcal{V}} H_{ij} \mathrm{d}\mathbf{r}_j \mathrm{d}\Omega_j} \mathrm{d}\mathbf{r}_i \mathrm{d}\Omega_i \\ &= 1 - \frac{\rho}{4\pi} \iint_{\mathcal{V}} e^{-\rho \mathsf{M}(\mathbf{r}_i)} \mathrm{d}\mathbf{r}_i \mathrm{d}\Omega_i. \end{aligned} \tag{15}$$

The density regime under which (15) is valid requires a similar analysis as that discussed for the isotropic case above. Note that for homogeneous domains, the ith node's position and orientation is arbitrary such that (15) simplifies to

$$P_{fc} = 1 - N e^{-\rho \mathsf{M}}, \tag{16}$$

where M is the *homogeneous connectivity mass defined through*

$$\mathsf{M} = \frac{1}{4\pi} \iint_{\mathbb{R}^3} H(|\mathbf{r}_j|) \mathrm{d}\mathbf{r}_j \mathrm{d}\Omega_j. \tag{17}$$

Significantly, in this case we have that the pair formation probability is simply $p_2 = H_i = \mathsf{M}/V$, and the mean degree is $\mu = \rho \mathsf{M}$ when $N \gg 1$. Furthermore, by comparing (16) to (13) it is clear that our expression for P_{fc} becomes an exponentially tight lower bound to $P_{md}(1)$ for large enough N and μ. This is intuitive since any fully connected network has minimum degree of at least 1. However, the opposite is not necessarily true. For instance a network comprising of two pairs of connected nodes has minimum degree 1 but is not fully connected. We will later numerically confirm this bound for a variety of antenna gain profiles (see Fig. 8).

In conclusion, we have presented strong evidence that the connectivity mass is a key observable of interest as it contains information about p_2, $d(k)$, μ, $P_{md}(k)$, and P_{fc}. It is worth noting that contrary to P_{fc}, $P_{md}(k)$ and $d(k)$, the pair formation probability p_2 and the mean degree μ are *local* observables involving only two nodes (rather than *global* ones involving $N \gg 1$ nodes[8]). Consequently, if the typical system size is much larger than the typical connectivity range r_0, we expect p_2 and μ to be very much insensitive to the domain shape details leading to $p_2 \lesssim \mathsf{M}/V$ and $\mu \lesssim \rho \mathsf{M}$. This is because H_i is approximately constant for the majority of node positions (away from the domain boundary) and orientations, and decreases (approximately linearly) when closer than $\sim r_0$ to the boundary. We will confirm this expectation later through computer simulations (see Fig. 7).

In this section we have argued that the connectivity mass is a key metric of network connectivity. We have achieved this by establishing direct links with a number of network observables. The physical significance of the connectivity mass is that it characterizes the local connectivity of a node. This local characteristic is then translated to a global one through the exponentiation of the connectivity mass in equations (10), (13) and (15). Our aim in what follows is to analyse and understand the connectivity mass for different anisotropic radiation patterns and thus offer intelligent and useful design

[7] Identifying at what densities (14) is valid requires further analysis beyond the scope of the current paper.

[8] Intuitively, this is why the position and orientation integrals of node j appear in the exponents of (10), (13) and (15).

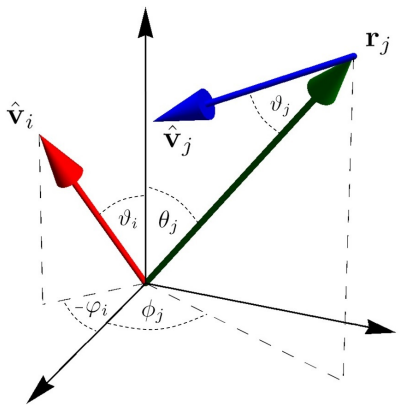

Fig. 2. Reference frame centred at $\mathbf{r}_i$. Assuming that the gain functions are rotationally symmetric, then G_j is a function of the angle between $\hat{\mathbf{v}}_j$ and $-\mathbf{r}_j$ given by ϑ_j, while G_i a function of the angle between $\hat{\mathbf{v}}_i$ and $\mathbf{r}_j$ given by $\chi = \arccos(\cos\theta_j\cos\vartheta_i + \cos(\phi_j - \varphi_i)\sin\theta_j\sin\vartheta_i)$. Note that when $\vartheta_i = 0$, then $\chi = \theta_j$.

recommendations which improve the connectivity of wireless communication networks. We begin with the case of a homogeneous system.

IV. Homogeneous Anisotropic Connectivity Mass

Since the system is homogeneous, we can choose $\mathbf{r}_i$ as the origin of the reference frame such that $r_{ij} = |\mathbf{r}_j|$ which we write as r_j for convenience. Furthermore, since the system is isotropic we can conveniently choose $\hat{\mathbf{v}}_i = (1, 0, 0)$ in spherical coordinates. The position coordinates of node j are given by $\mathbf{r}_j = (r_j, \theta_j, \phi_j)$, while its orientation by $\hat{\mathbf{v}}_j = (1, \vartheta_j, \varphi_j)$ as shown in Fig. 2. Note that since the gain functions are rotationally symmetric, φ_j is a free parameter.

In the analysis that follows we will assume only small scale scattering effects and thus adopt a *Rayleigh fading* model[9] where $|h|^2$ in (1) is modelled as an exponentially distributed random variable [25]. The pair connectedness function is therefore given by

$$H_{ij} = \exp\left(-\frac{\beta r_j^\eta}{G_i(\theta_j)G_j(\vartheta_j)}\right), \tag{18}$$

where β depends on for example the transmission wavelength, signal power, *et cetera*, and defines an effective communication range $r_0 = [\beta/(G_iG_j)]^{-1/\eta}$ between nodes i and j. Significantly, in the limit of $\eta \to \infty$, the connection probability H_{ij} is no longer probabilistic but rather converges to the deterministic hard-disk model with an *on/off* communication range at r_0. Notice that G_i is a function of the position of j whilst G_j is a function of the orientation of antenna j as described in the caption of Fig. 2. Performing the r_j, ϕ_j and φ_j integrals in (17) and simplifying we arrive at our first main result

$$\begin{aligned}\mathsf{M} &= \frac{1}{4\pi}\int\!\!\int_0^{2\pi}\int_0^{\pi}\int_0^{\infty} r_j^2\sin\theta_j H_{ij}\mathrm{d}r_j\mathrm{d}\theta_j\mathrm{d}\phi_j\mathrm{d}\Omega_j \\ &= \frac{\pi\Gamma(3/\eta)}{\eta\beta^{3/\eta}}\left(\int_0^{\pi}\sin\theta_j G_i(\theta_j)^{3/\eta}\mathrm{d}\theta_j\right)\left(\int_0^{\pi}\sin\vartheta_j G_j(\vartheta_j)^{3/\eta}\mathrm{d}\vartheta_j\right)\end{aligned} \tag{19}$$

where $\Gamma(x)$ is the gamma function and the separation of the integrals is analogous to that obtained in the 2D case [16]. We notice that when $\eta = 3$, the homogeneous connectivity mass M is invariant[10] with respect to the specific radiation pattern due to the normalization condition in (3). Therefore, in 3D we expect the ratio $3/\eta$ to be a key system parameter dictating the performance of M for different antenna gain profiles. Generalizing this to arbitrary $d \geq 2$ dimensional domains is straight forward and results in angular integrals involving $G^{d/\eta}$ such that M becomes invariant with respect to G when $d = \eta$.

Since the gain integrals in (19) of G_i and G_j factor out nicely and are equivalent to each other, we define

$$S_\eta[G] = \int_0^{\pi}\sin\theta G(\theta)^{3/\eta}\mathrm{d}\theta, \tag{20}$$

and investigate the functional's dependence with respect to the path exponent η, for simple but practical gain functions in order to identify which ones yield better (or worse) connectivity properties.

A. Isotropic Radiation

As a benchmark for our theoretical analysis we set $G = 1$ corresponding to isotropic radiation. In this case we have the following trivial result for the functional of interest

$$S_\eta[G] = \int_0^{\pi}\sin\theta\mathrm{d}\theta = 2. \tag{21}$$

B. Wide-Angle Unidirectional Radiation

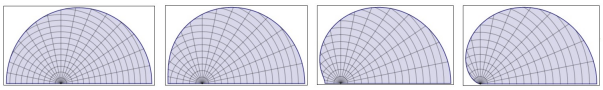

Fig. 3. The cardioid pattern for $\epsilon = 1/4, 1/2, 3/4$, and 1, from left to right.

Wide-angle unidirectional radiation patterns are characteristic of microstrip antennas, also called patch antennas. Patch antennas are relatively cheap and easy to manufacture using modern printed-circuit technology. Moreover, they are mechanically robust and therefore are generally used in wireless communications where size, weigh, cost, performance, and ease of installation are often the main constraints [26]. Their narrow bandwidth is being somewhat mitigated by the fact that many communications protocols are nowadays moving towards CDMA and TDMA techniques which use a single band.

[9]More exotic fading models such as the two-wave with diffuse power (TWDP) [24] which can approximate channels with arbitrary combinations of specular and diffuse components, offer little additional insight to the present discussion as our approach will be concentrated on the antenna radiation patterns rather than the detailed fading parameters [16].

[10]A similar observation was made for two dimensional domains in [16] where the critical path loss was found to be $\eta = 2$.

Patch antenna gains typically have a single wide-angled major lobe with a number of small minor ones. We ignore the minor lobes and approximate the patch antenna radiation pattern by the cardioid function $G(\theta) = 1 + \epsilon\cos\theta$, for $\theta \in (0, \pi)$ with $\epsilon \in [0, 1]$. The parameter ϵ measures the extent of deformation from the isotropic case as shown in Fig. 3 with $\epsilon = 1$ corresponding to the most directional case. To obtain the 3D radiation pattern, the gain profile of Fig. 3 is rotated about the x-axis, thus producing a surface of revolution. For general ϵ we find

$$S_\eta[G] = \eta\frac{(1+\epsilon)^{1+3/\eta} - (1-\epsilon)^{1+3/\eta}}{\epsilon(\eta+3)}. \quad (22)$$

Notice that when $\epsilon = 0$ we recover (21), whilst when $\epsilon = 1$ we have $S_\eta[G] = \frac{2^{1+3/\eta}}{1+3/\eta}$.

C. Omnidirectional Radiation

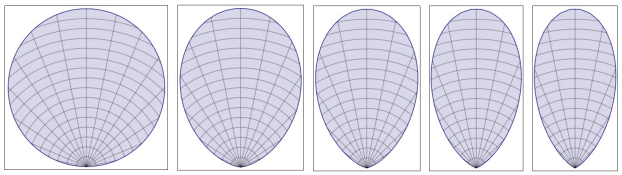

Fig. 4. The donought pattern for $m = 1, \ldots, 5$, from left to right.

Omnidirectional radiation patterns are characteristic of dipole antennas, commonly used in wideband wireless applications. Their radiation pattern is shaped like a doughnut and is symmetric about the axis of the dipole. In the simplest case of a half-wavelength dipole antenna we may approximate this pattern by $G(\theta) = \frac{2\Gamma(\frac{3+m}{2})}{\sqrt{\pi}\Gamma(\frac{2+m}{2})}\sin^m\theta$, for $\theta \in (0, \pi)$ with $m > 0$ [26]. The parameter m measures the directivity of the donought ring as shown in Fig. 4. For general m we find

$$S_\eta[G] = \left(\frac{2\Gamma(\frac{3+m}{2})}{\sqrt{\pi}\Gamma(\frac{2+m}{2})}\right)^{3/\eta}\frac{\sqrt{\pi}\Gamma(1+\frac{3m}{2\eta})}{\Gamma(\frac{3(m+\eta)}{2\eta})}. \quad (23)$$

D. Narrow-Angle Unidirectional Radiation

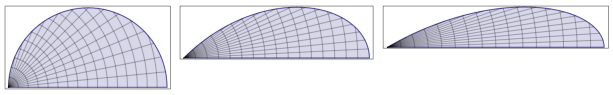

Fig. 5. The highly directional horn pattern for $\lambda = 1, 2, 3$, from left to right.

Highly directional patterns are characteristic of horn antennas and can also be generated by end-fire arrays. Typical applications include high powered satellite communications and radio telescopes, although beamforming techniques have recently attracted much attention in low-power wireless multihop networks [13], [15]. We approximate their radiation pattern by $G(\theta) = (2(\lambda^2-1)\cos\lambda\theta)/(\lambda\sin\frac{\pi}{2\lambda} - 1)$ in the interval $\theta \in (0, \frac{\pi}{2\lambda})$ with for $\lambda \geq 1$ and $G = 0$ elsewhere. The parameter λ measures the directivity of the beam as shown in Fig. 5. For the case of $\lambda = 2$ we find

$$S_\eta[G] = \frac{\eta(6+6\sqrt{2})^{3/\eta}}{2(3+\eta)}{}_2F_1(1, \frac{3}{2}+\frac{3}{\eta}, 2+\frac{3}{\eta}, -1), \quad (24)$$

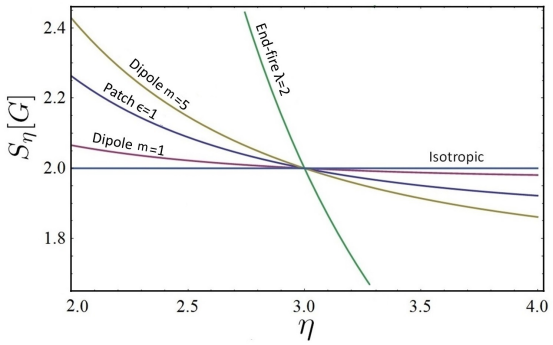

Fig. 6. Comparison of the functional $S_\eta[G]$ as a function of the path loss exponent η for the various radiation patterns considered in this section. Directional radiation patterns are superior to the isotropic case only when $\eta < 3$.

where ${}_2F_1$ is the Gauss hypergeometric function. Closed form expressions exist for other values of λ but become increasingly complicated and do not offer further insight.

E. Narrow-Angle Multi-directional Radiation

As a generalization to the above unidirectional radiation pattern we allow for the possibility of multiple, non-overlapping, highly directional, identical lobes (see the left panel of Fig. 9 for an example with $n = 6$ lobes). Although such exotic gain patterns are not often encountered in practice[11], the following theoretical investigation presents an interesting exercise and can offer some useful design recommendations. For a radiation pattern with $n > 1$, the gain function is given by (4) with each lobe described by $g_k(\theta^{(k)}) = (2(\lambda^2-1)\cos\lambda\theta^{(k)})/(n\lambda\sin\frac{\pi}{2\lambda} - n)$ for $k = 1, \ldots, n$, with $\theta^{(k)} \in (0, \frac{\pi}{2\lambda})$, and $\lambda \geq 1$. For the case of $\lambda = 2$ and general n we find

$$\begin{aligned} S_\eta[G] &= \sum_{k=1}^{n}\int_0^{\frac{\pi}{2\lambda}}\sin(\theta^{(k)})g_k(\theta^{(k)})^{3/\eta}\mathrm{d}\theta^{(k)} \\ &= \frac{n^{1-3/\eta}\eta(6+6\sqrt{2})^{3/\eta}}{2(3+\eta)}{}_2F_1(1, \frac{3}{2}+\frac{3}{\eta}, 2+\frac{3}{\eta}, -1), \end{aligned} \quad (25)$$

where we have assumed no overlapping lobes and thus considered each lobe's contribution to the integral individually. Notice that for $\eta < 3$, increasing the number of lobes n, *ceteris paribus*, has the effect of decreasing $S_\eta[G]$. This is particularly interesting since it implies for example that at low path loss ($\eta = 2$) and identical receive and transmit gains (i.e. $G_i = G_j$), doubling the number of lobes (normalized at constant total power (3)) would result to halving the network mean node degree μ. Similarly, at high path loss ($\eta = 6$), doubling the number of lobes doubles μ.

F. Single Sector Radiation

To simplify matters, we also consider a sectorized radiation model [19], [28] where $G(\theta) = f(\nu) = \text{const} > 0$ for the

[11] Experimental realizations of multi-directional radiation patterns have reported substantial benefits and point towards successful application to large-scale wireless sensor networks [27].

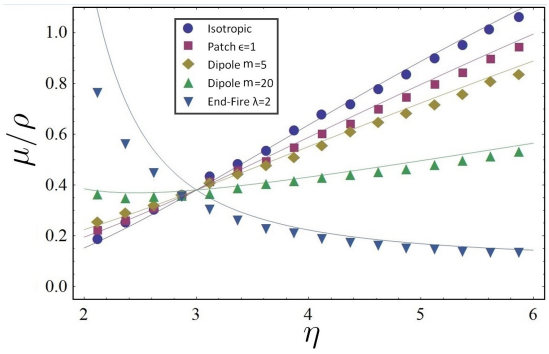

Fig. 7. Comparison of the computer simulated mean degree μ (showing using solid markers) and the theoretical prediction (curved line) for different antenna gains and for a range of path loss values $\eta \in [2, 6]$. The simulation was run in a cube domain of side $L = 10$, at a density $\rho = 0.1$ and $\beta = 10$.

interval $\theta \in (0, \nu\pi)$ for some $\nu \leq 1$ and $G = 0$ elsewhere. This would result in a conical radiation pattern ending in a spherical cap. In complete analogy to the 2D case [16], by employing Lagrange multipliers in the calculus of variations we find that the constant gain function $G(\theta) = \csc^2(\frac{\nu\pi}{2})$ yields the stationary path of $S_\eta[G]$. For general ν we find

$$S_\eta[G] = 2\left[\sin\left(\frac{\nu\pi}{2}\right)\right]^{2-\frac{6}{\eta}}, \tag{26}$$

implying that the path defined by the isotropic radiation gain (i.e. when $\nu = 1$) is a maximum of $S_\eta[G]$ for $\eta > 3$, and a minimum for $\eta < 3$. Therefore, we may conclude that isotropic radiation offers optimal connectivity properties when $\eta > 3$ but the worst possible when $\eta < 3$.

G. Numerical Verification and Discussion

Fig. 6 provides a qualitative comparison of $S_\eta[G]$, and thus M, for the various gain functions considered above. It is clear that directional radiation patterns can significantly improve network connectivity in 3D homogeneous domains at low path loss $\eta < 3$. This observation is in good agreement with the numerical results in two dimensional networks of [15], [29], yet further highlights the importance of the ratio d/η as well as its generality to any directional antenna gain profile or small-scale fading model. Significantly, equation (19) suggests that homogeneous networks with antennas which have different receive and transmit gains, for example directional transmit but isotropic receive gains (often adopted to avoid antenna misalignments) are in fact in great disadvantage to directional-directional for $\eta < 3$ and isotropic-isotropic for $\eta > 3$. This is an important and generic observation which is independent of i) the gain pattern details (e.g. minor lobes or sectorized approximation), ii) the fading model used, and should therefore be contrasted against the multitude of related research works (see [30]–[32] and references therein).

In order to validate our results thus far, we compare theoretical predictions with numerical results obtained through computer simulations. In the simulations, spatial and orientation coordinates for N nodes are chosen independently at random inside a particular domain defined by $\mathcal{V}$. The nodes are then paired up whenever a randomly generated number $\zeta \in [0, 1] \leq H_{ij}$. This guarantees that the links between pairs of nodes are statistically independent. We store the resulting graph connections in a symmetric adjacency matrix from which we can extract various observable of interest e.g. the mean degree or whether the graph is fully connected. In order to improve our statistics, the above process is then repeated in a Monte Carlo fashion.

Figure 7 shows a comparison between theory and computer simulations. The observable of choice is the mean degree μ of a random network with randomly oriented antennas at different path loss values within the range of $\eta \in (2, 6)$. Note that in Fig. 7 we divide μ by ρ since for $V \gg 1$, the mean degree increases linearly with the number of nodes in the network. This allows for a direct comparison with the theoretical prediction of the homogeneous connectivity mass M. The simulation confirms that at $\eta = 3$ all curves meet and the mean degree is independent of the gain pattern details. A good agreement is observed between theory and simulation, although the theoretical curve appears to systematically overestimate that of the simulation data. The reason for this is that the numerical simulation was performed in a finite cube domain (of side length $L = 10$) therefore inducing boundary effects, which have thus far been ignored in the theoretical model under the assumption of a homogeneous system. Therefore, in the numerical simulations, nodes near the boundary may occasionally steer their main beam outside of the domain and are typically of lower degree. While this phenomenon applies to all directional patterns, it is most significant when the gain is concentrated over a narrow solid angle. Indeed, the curve for the highly directional end-fire radiation pattern is noticeably above that of the data at low path loss $\eta < 3$. We elaborate on this further in Sec. VI.

Figure 8 also shows a comparison between theory and computer simulations. Unlike in Fig. 7, here the simulations intentionally ignore boundary effects by not using statistics drawn from nodes near the borders of the domain. Similar numerical methods have been used in the literature (see for example [13]). The observable of choice in Fig. 8 is $P_{md}(1)$ i.e. the probability that all nodes have degree greater or equal to 1. We perform the simulations for three types of antenna gain patterns and for $\eta = 2$ and $\eta = 4$. Notice that the more directional the antennas are the better connected the network is for $\eta < 3$, and *vice versa* fro $\eta > 3$. We also plot the analytical predictions from (13) using solid curves, and those of (15) using dashed curves. An excellent agreement is observed between theory and computer simulations. It is also clear that the expression for P_{fc} (dashed curves) diverges from $P_{md}(1)$ at lower densities but is a tight lower bound in at high enough densities.

V. Directivity Scaling

Expressions (23), (24) and (26) have highly directional limits, for $m \to \infty$, $\lambda \to \infty$, and $\nu \to 0$ respectively, in which the gain pattern and derived quantities scale. Physically we see that if the gain G is concentrated on a small solid angle ω, hence (due to normalisation) having values of order ω^{-1}, the integral $S_\eta[G]$ will scale as $\omega^{1-3/\eta}$. We can see this

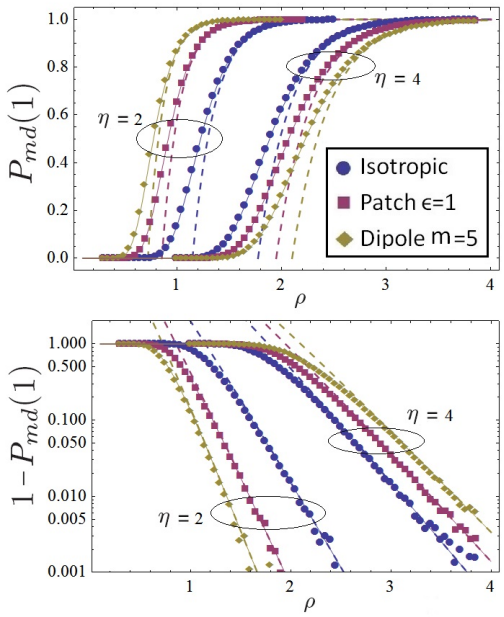

Fig. 8. *Top:* Comparison of numerical simulations of $P_{md}(1)$ (markers) with the analytical prediction of (13) (solid curves). The numerical simulations are performed in a homogeneous domain (i.e. ignoring boundary effects) using $\beta = 1$ for three different antenna radiation patterns and for $\eta = 2$ and $\eta = 4$. The dashed curves correspond to the analytical prediction of P_{fc} as defined in (15). *Bottom:* Same as above but $1 - P_{md}(1)$ is plotted on a log-linear scale thus highlighting the excellent agreement between simulation and theory at high node densities.

in more detail for each of the two models. Define ω to be the solid angle over which G takes at least half its maximum value. Then for the dipole case of $G(\theta) = \frac{2\Gamma(\frac{3+m}{2})}{\sqrt{\pi}\Gamma(\frac{2+m}{2})}\sin^m\theta$, we require that $\sin^m\theta \geq 1/2$, which gives a small interval (to leading order in m^{-1}): $|\theta - \pi/2| \leq \sqrt{2\ln 2/m}$. Multiplying the width of this interval $2\sqrt{2\ln 2/m}$ by the length of the equator 2π gives

$$\omega = \sqrt{\frac{32\pi^2 \ln 2}{m}}, \tag{27}$$

for $m \to \infty$. Applying the asymptotic formula for the ratio of gamma functions in (23) $\frac{\Gamma(z+a)}{\Gamma(z+b)} \sim z^{a-b}$, (see [33] 5.11.12) for $z \to \infty$ and comparing with (27) we find that

$$S_\eta[G] \sim C_1(\eta)\omega^{1-3/\eta}, \tag{28}$$

for an explicit (but rather unilluminating) function $C_1(\eta)$.

For the highly directional radiation pattern $G(\theta) = (2(\lambda^2 - 1)\cos\lambda\theta)/(\lambda\sin\frac{\pi}{2\lambda} - 1)$ for $\theta \in (0, \frac{\pi}{2\lambda})$, we use the same definition of ω, this time finding $\theta \leq \pi/(3\lambda)$ and hence

$$\omega = 4\pi\sin^2\left(\frac{\pi}{2\lambda}\right) \sim \frac{\pi^3}{9\lambda^2}. \tag{29}$$

Making a change of variable $t = \lambda\theta$ in the integral of interest, we find

$$S_\eta[G] = \left(\frac{2(\lambda^2-1)}{\lambda\sin(\pi/2\lambda) - 1}\right)^{3/\eta} \int_0^{\pi/2} \frac{\sin(t/\lambda)\cos^{3/\eta} t}{\lambda}\mathrm{d}t. \tag{30}$$

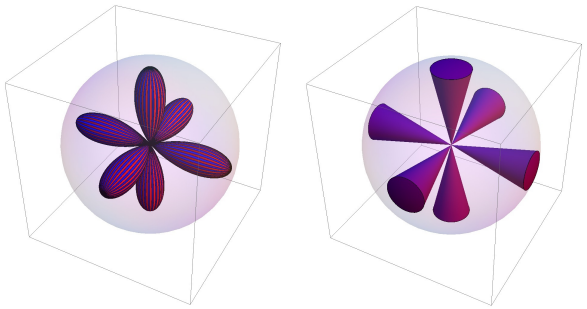

Fig. 9. An example of a narrow-angled multi-directional radiation pattern with $n = 6$ evenly spaced non-overlapping lobes is shown on the left with its corresponding multi-sectorized approximation on the right.

Taking the limit $\lambda \to \infty$, the sines take their forms for small argument, and so

$$\begin{aligned} S_\eta[G] &\sim \left(\frac{2}{\pi/2 - 1}\right)^{3/\eta} \lambda^{6/\eta - 2} \int_0^{\pi/2} t\cos^{3/\eta} t\,\mathrm{d}t \\ &\sim C_2(\eta)\omega^{1-3/\eta}, \end{aligned} \tag{31}$$

where now $C_2(\eta)$ involves a non-elementary integral for most values of η.

Finally, for the single sector radiation pattern we have that in the directional limit of $\nu \to 0$, equation (26) becomes

$$\begin{aligned} S_\eta[G] &\sim 2\left(\frac{\nu\pi}{2}\right)^{2-\frac{6}{\eta}} \\ &\sim 2^{\frac{3}{\eta}}\left(\frac{\omega}{2\pi}\right)^{1-\frac{3}{\eta}}, \end{aligned} \tag{32}$$

since $\omega = 2\pi(1 - \cos\nu\pi) = \pi^3\nu^2 + \mathcal{O}(\nu^4)$.

Significantly, we find that when $G_i = G_j$, in either of the above three cases cases the connectivity mass scales as $\mathsf{M} \sim C_3(\eta)\omega^{2-6/\eta}$. Thus when $\eta < 3$, scaling the density as $\rho \sim \omega^{6/\eta-2}$ will keep the exponent $\rho\mathsf{M}$ in (16) constant but result in a decrease in N, and hence lead to an increase in the probability of full connectivity. For example, when $\eta = 2$, this suggests that by making a directional beam of half the solid angle, we may reduce the number of nodes by a significant factor of 2 without affecting M or any of the associated network connectivity properties described in Sec. III. We conclude this section by noting that it is reasonable to expect our results to generalize to any dimension $d \geq 2$ such that $\mathsf{M} \sim \omega^{2-2d/\eta}$.

VI. Inhomogeneous Anisotropic Connectivity Mass and Boundary Effects

Random networks confined within a bounded domain $\mathcal{V} \subset \mathbb{R}^3$ are no longer homogeneous nor isotropic. As a result, boundary effects can have a significant impact on the connectivity properties of such networks [23], [34]–[37]. The main reason behind this is that nodes situated near the boundary have a higher probability of being isolated (i.e. of degree 0) than nodes in the bulk component of $\mathcal{V}$. This feature is quantified by (14) in the isotropic case, and further intensified in the case of anisotropic radiation patterns where nodes near the boundary may steer their connectivity beam(s) outside the network domain and hence increase their isolation likelihood.

Therefore, unlike in homogeneous systems where directivity significantly improves network connectivity at low path loss, in inhomogeneous systems, directional radiation patterns present us with some serious drawbacks.

In order to understand the negative effects of directional radiation patterns, we restrict the current investigation to rotationally symmetric gain patterns (i.e. we exclude multi-directional antennas) and also consider boundary effects due to a right angled corner[12] (i.e. where three planes meet and are normal to each other.). We naturally choose the corner as the origin of the reference frame, with the corner edges aligned with the positive coordinate axes. Note that the system is not isotropic and so G_i is a function of the angle between $\hat{\mathbf{v}}_i$ and $\mathbf{r}_j$ given by $\chi = \arccos(\cos\theta_j \cos\vartheta_i + \cos(\phi_j - \varphi_i)\sin\theta_j \sin\vartheta_i)$ as illustrated in Fig. 2. We therefore have that the connectivity mass of a node situated at the corner denoted here by $\mathsf{M}_C = \mathsf{M}(\mathbf{0}, \hat{\mathbf{v}}_i)$ is given by

$$\begin{aligned}\mathsf{M}_C &= \frac{1}{4\pi}\int\!\!\int_0^{\frac{\pi}{2}}\int_0^{\frac{\pi}{2}}\int_0^{\infty} r_j^2 \sin\theta_j e^{-\frac{\beta r_j^\eta}{G_i(\chi)G_j(\vartheta_j)}} \mathrm{d}r_j \mathrm{d}\theta_j \mathrm{d}\phi_j \mathrm{d}\Omega_j \\ &= \frac{\Gamma(3/\eta)}{4\pi\eta\beta^{3/\eta}}\int\!\!\int_0^{\frac{\pi}{2}}\int_0^{\frac{\pi}{2}} \sin\theta_j (G_i(\chi)G_j(\vartheta_j))^{3/\eta} \mathrm{d}\theta_j \mathrm{d}\phi_j \mathrm{d}\Omega_j \\ &= \frac{\Gamma(3/\eta)}{2\eta\beta^{3/\eta}}\left(\int_0^{\frac{\pi}{2}}\int_0^{\frac{\pi}{2}} \sin\theta_j G_i(\chi)^{3/\eta} \mathrm{d}\theta_j \mathrm{d}\phi_j\right) S_\eta[G_j],\end{aligned} \tag{33}$$

where we have extended the radial integral in the first line of (33) to infinity (even though $\mathcal{V}$ is finite) since H_{ij} is decaying exponentially - a reasonable approximation if the effective communication range r_0 is much smaller than the size of the system.

It is important to note that unlike the homogeneous case where the connectivity mass was invariant to the gain details at $\eta = 3$, in (33), M_C depends strongly on G_i through the antenna orientation $\hat{\mathbf{v}}_i$ of the cornered node i for all values of η. Therefore, we define the functional

$$I_{G_i}(\vartheta_i, \varphi_i) = \int_0^{\frac{\pi}{2}}\int_0^{\frac{\pi}{2}} \sin\theta_j G_i(\chi)^{3/\eta} \mathrm{d}\theta_j \mathrm{d}\phi_j \tag{34}$$

and seek it's minimum value with respect to the orientation vector $\hat{\mathbf{v}}_i$ resulting in the minimum connectivity mass orientation at a right angled corner which we define here as

$$\mathcal{M} = \min_{\hat{\mathbf{v}}_i} \mathsf{M}_C. \tag{35}$$

When M_C is at it's minimum, node i is likely to have low (or zero) degree thus affecting both local and global network properties such as μ and P_{fc} respectively.

A. Isotropic Radiation

In this case $G = 1$ and we obtain the trivial result that $I_{G_i} = \pi/2$ and so $\mathcal{M} = \mathsf{M}_C = \frac{\Gamma(3/\eta)\pi}{2\eta\beta^{3/\eta}}$. More generally, for a corner of solid angle ω_C we would have $\mathcal{M} = \mathsf{M}_C = \frac{\Gamma(3/\eta)}{\eta\beta^{3/\eta}}\omega_C$.

[12]Without this assumption all the results generalize but exposition and notations become a little more cumbersome.

B. Wide-Angle Unidirectional Radiation

In this case, $G(\theta) = 1 + \epsilon\cos\theta$, which leads to a global minimum in (34) at $(\vartheta_i, \varphi_i) = (\pi - \theta_j, \phi_j + \pi)$, i.e. when $\mathbf{r}_i = -c\hat{\mathbf{v}}_i$ for any $c > 0$ which can only occur if $\hat{\mathbf{v}}_i$ is pointing outside of $\mathcal{V}$. Such a configuration amounts to

$$I_{G_i}(\pi - \theta_j, \phi_j + \pi) = \frac{\pi}{2}(1 - \epsilon)^{3/\eta}. \tag{36}$$

Note that when $\epsilon = 1$, we have that $I_{G_i} = 0$ which is indicative of a blind spot, meaning that any node directly behind node i finds it impossible to connect with it. However such a configuration is highly unlikely as it is of zero probability measure.

C. Omnidirectional Radiation

In this case, $G(\theta) = \frac{2\Gamma(\frac{3+m}{2})}{\sqrt{\pi}\Gamma(\frac{2+m}{2})}\sin^m\theta$, which leads to two global minima in (34) at $(\vartheta_i, \varphi_i) = (\pi - \theta_j, \phi_j + \pi)$ and $(\vartheta_i, \varphi_i) = (\theta_j, \phi_j)$, giving $I_{G_i} = 0$ in both cases. This is expected due to the zero gain in both $\pm\hat{\mathbf{v}}_i$ directions, however as with the previous case, such a configuration is highly unlikely.

D. Narrow-Angled Unidirectional Radiation

In this case, $G(\theta) = (2(\lambda^2 - 1)\cos\lambda\theta)/(\lambda\sin\frac{\pi}{2\lambda} - 1)$, which leads to $I = 0$ for a range of orientations independent of (θ_j, ϕ_j), i.e. whenever the entire lobe is oriented outside of the domain $\mathcal{V}$. Therefore, the blind-spot phenomenon is much more likely. For this reason, we conclude that while highly directional antennas improve connectivity in homogeneous domains at low path loss, they are in some disadvantage to wide-angle unidirectional or omnidirectional antennas in inhomogeneous domains.

VII. Inhomogeneous Connectivity Mass for Multi-directional Radiation

Networks operating in homogeneous environments at low path loss can improve their connectivity by using highly directional antennas. Networks operating in inhomogeneous domains however suffer from boundary effects (especially near sharp corners) where nodes with unidirectional radiation patterns (and especially narrow-angle ones) may steer their main beam outside the domain thus suffering from blind-spots. In the absence of any *a posteriori* knowledge or control over antenna orientations (e.g. beamstearing capabilities) it is therefore desirable to identify ways of mitigating blind-spots in order to achieve high connectivity mass both near and away from the domain boundary.

One possible approach to the above stated problem is to consider multi-directional patterns where the gain is concentrated on $n \geq 2$ *evenly spaced* lobes. Similar radiation patterns have been experimentally realized in [27] using a number of patch antennas. Since we are interested in the performance of G in low path loss we now lift the assumption that the connectivity range is much smaller than the size of the system[13].

[13]Recall that this assumption was used to extend the radial integral of (33) to infinity.

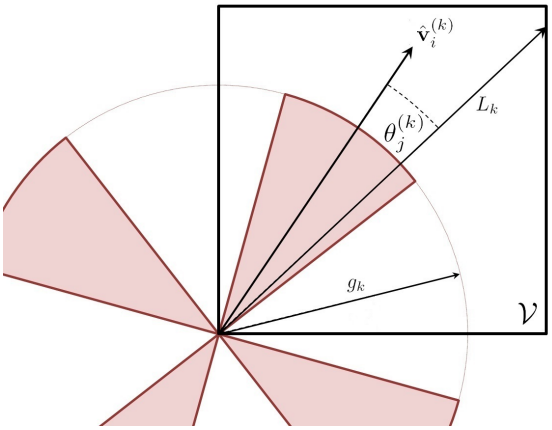

Fig. 10. Schematic of a multi-directional gain pattern ($n = 4$) of a node situated at one of the corners of a square domain.

A. Two Dimensional Case

In order to aid in the discussion of the impact of boundaries in 3D multi-directional radiation patterns, we first discuss the 2D case. In two dimensions, distributing $n \geq 2$ points evenly on the unit circle is a trivial problem with $\Theta = \{\hat{\mathbf{v}}^{(k)} = (1, 2\pi k/n + x),$ for $k = 1, \ldots, n$ and $x \in [0, 2\pi/n)\}$. Each lobe has $g_k(\theta^{(k)}) = \lambda\pi \cos\lambda\theta$ for $\theta \in (-\frac{\pi}{2\lambda}, \frac{\pi}{2\lambda})$ and $\lambda \geq 1$, and the total gain profile G is defined by (4). Following the discussion in Sec. V, we may simplify the multi-directional gain function for $\lambda \gg 1$ by considering a multi-sectorized radiation model where each 2D lobe is approximated by a sector of angular width $\omega = 2\pi/(3\lambda)$ and gain $g_k(\theta^{(k)}) = 3\lambda/n$ for $\theta^{(k)} \in (-\frac{\pi}{3\lambda}, \frac{\pi}{3\lambda})$ measured from $\hat{\mathbf{v}}^{(k)}$ and 0 otherwise, such that the total power is normalized by

$$\int_0^{2\pi} G(\theta)\mathrm{d}\theta = \sum_{k=1}^{n} \int_{-\frac{\pi}{3\lambda}}^{\frac{\pi}{3\lambda}} g_k(\theta^{(k)})\mathrm{d}\theta = 2\pi. \tag{37}$$

Also, to avoid overlap between lobes we require that $\lambda \geq 3n$.

Having defined G, we now examine the two dimensional multi-directional analogue of (35) given by $\mathcal{M}(n) = \min_x \mathsf{M}_C(n)$, for a right angled corner of a square domain $\mathcal{V} \subset \mathbb{R}^2$. The contribution to $\mathsf{M}_C(n)$ from a single sector of antenna i is given by

$$\frac{n}{2\pi} \int_{-\frac{\pi}{3\lambda}}^{\frac{\pi}{3\lambda}} \int_{-\frac{\pi}{3\lambda}}^{\frac{\pi}{3\lambda}} \int_0^{L_k} r_j \exp\left(\frac{-\beta r_j^\eta}{g_k(\theta^{(k)})^2}\right) \mathrm{d}r_j \mathrm{d}\theta_j^{(k)} \mathrm{d}\vartheta_j, \tag{38}$$

where the factor of n in the front is due to the n lobes of antenna j, and L_k is the radial distance from the corner to the adjacent boundary of $\mathcal{V}$ in the direction $\theta_j^{(k)}$ measured from $\hat{\mathbf{v}}_i^{(k)}$, as illustrated for $n = 4$ in Fig. 10. Performing the $\mathrm{d}r_j$ integral and summing over k we obtain

$$\mathsf{M}_C(n) = \frac{n g^{4/\eta}}{2\pi\eta\beta^{2/\eta}} \sum_{k=1}^{n} \int_{-\frac{\pi}{3\lambda}}^{\frac{\pi}{3\lambda}} \int_{-\frac{\pi}{3\lambda}}^{\frac{\pi}{3\lambda}} \gamma\left(\frac{2}{\eta}, \frac{\beta L_k^\eta}{g^2}\right) \mathrm{d}\theta_j^{(k)} \mathrm{d}\vartheta_j, \tag{39}$$

where $\gamma(s, x)$ is the lower incomplete gamma function. Note that we have dropped the subscript k from g as all lobes are identical. For highly directional sectors ($\lambda \gg 1$), we may approximate L_k by $\hat{L}_k$ given by the length of the vector $\hat{\mathbf{v}}_i^{(k)}$ projected onto the adjacent boundary of $\mathcal{V}$. Notice that $\hat{L}_k$ is zero if the lobe is pointing outside the domain. After some simplifications we finally arrive at

$$\mathcal{M}(n) \approx \min_x \left[\frac{2\pi g^{4/\eta - 2}}{n\eta\beta^{2/\eta}} \sum_{k=1}^{n} \gamma\left(\frac{2}{\eta}, \frac{\beta \hat{L}_k^\eta}{g^2}\right) \right], \tag{40}$$

indicating that the finite size effect of truncating radial integration at $\hat{L}_k$ is of variable importance at different path loss. Equation (40) is difficult to calculate analytically, but straightforward numerically using a fine grid of values for $x \in [0, 2\pi/n)$. We now turn to the full problem in three dimensions.

B. Three Dimensional Case

In three dimensions, there are a number of ways of arranging $n > 2$ points evenly on the unit sphere. One way is through the *Thomson problem* (proposed in 1904 by J.J. Thomson, see [38] and references therein) concerning the minimum energy configuration of n electrons confined on the surface of a sphere which repel each other with a Coulomb force. Other ways involve packing and covering problems called the Tammes and Fejes Tóth type problems respectively. We will adopt the Thomson interpretation for its connection with spherical molecule symmetries.

An analytic description of the n-point coordinate configuration is impossible. However, computer programs have generated them to very good accuracy and have also identified their symmetry types for very large values of n. One can try to imagine such configurations as the vertices of a polyhedron whose $2(n-2)$ faces are *almost* equilateral triangles[14]. An extensive table with the minimal energy, group symmetry, dual polyhedron and Cartesian coordinates of the n vertices can be found online at [39].

We consider a multi-sectorized radiation model where each lobe is approximated by a cone ending in a spherical cap of radius $g_k = \frac{1}{n}\csc^2(\frac{\pi}{6\lambda})$, each of solid angle $\omega = 4\pi \sin^2(\frac{\pi}{2\lambda})$ as in (29), thus satisfying the normalization condition (3). Fig. 9 shows an example multi-sectorized radiation model with $n = 6$. Notice that the resulting multi-directional gain pattern is not rotationally symmetric and so in general we have $\Theta = \{\hat{\mathbf{v}}^{(k)} = (1, \vartheta^{(k)}, \varphi^{(k)}),$ for $k = 1, \ldots, n\}$. Finally, using $\sqrt{4\pi/n}$ as a rough estimate of the typical angular distance between neighbouring lobes we require $\lambda \geq \sqrt{n\pi}/3$ to keep lobes from overlapping.

Having defined G, we now examine the connectivity mass $\mathsf{M}_C(n)$ associated with a right angled corner of a cube domain $\mathcal{V} \subset \mathbb{R}^3$. Taking the same approach as in the two dimensional

[14]For $n = 4, 6,$ and 12, the triangles are perfect equilaterals and so the polyhedrons formed are the regular tetrahedron, octahedron, and icosahedron respectively.

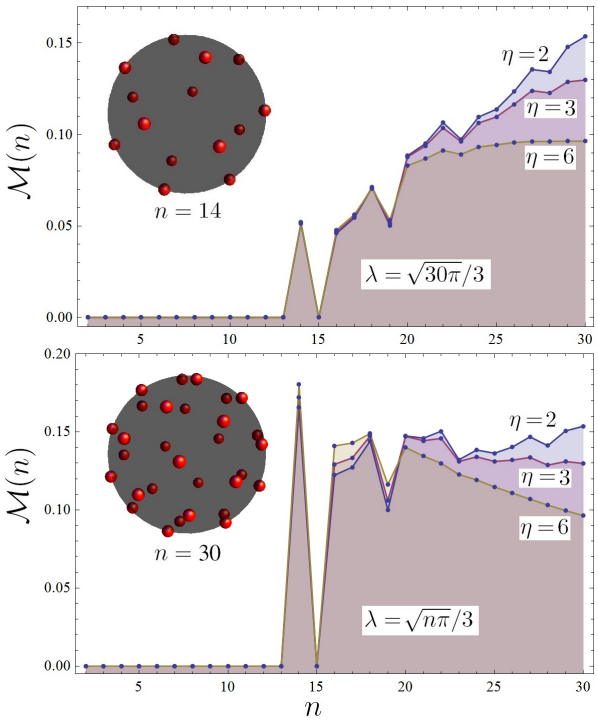

Fig. 11. Numerical calculation of the minimum connectivity mass (43) due to a multi-directional antenna situated at right angled corner for $\eta = 2, 3,$ and 6. The n evenly spaced vertex coordinates were taken from [39], and the minimum is taken over all possible orientations Θ_i using rotation matrices and a finite grid of Euler angles. The top panel keeps the lobe widths constant while the lower one shrinks them for increasing n by scaling λ by $\sqrt{n\pi}/3$. The insets show the vertex positions for $n = 14$ and $n = 30$.

case, we calculate

$$\begin{aligned}\mathsf{M}_C(n) &= \frac{n}{4\pi}\sum_{k=1}^{n}\iint_0^{2\pi}\int_0^{\frac{\pi}{3\lambda}}\int_0^{L_k} r_j^2 \sin\theta_j e^{-\beta\frac{r_j^\eta}{g^2}}\mathrm{d}r_j\mathrm{d}\theta_j\mathrm{d}\phi_j\mathrm{d}\Omega_j \\ &= \frac{ng^{6/\eta}}{4\pi\eta\beta^{3/\eta}}\sum_{k=1}^{n}\iint_0^{2\pi}\int_0^{\frac{\pi}{3\lambda}}\gamma\left(\frac{3}{\eta},\frac{\beta L_k^\eta}{g^2}\right)\sin\theta_j\mathrm{d}\theta_j\mathrm{d}\phi_j\mathrm{d}\Omega_j \\ &= \frac{g^{6/\eta-1}}{\eta\beta^{3/\eta}}\sum_{k=1}^{n}\int_0^{2\pi}\int_0^{\frac{\pi}{3\lambda}}\gamma\left(\frac{3}{\eta},\frac{\beta L_k^\eta}{g^2}\right)\sin\theta_j\mathrm{d}\theta_j\mathrm{d}\phi_j,\end{aligned} \tag{41}$$

where we have restricted the $\mathrm{d}\Omega_j$ integral over $\vartheta_j \in (0, \frac{\pi}{3\lambda})$ and $\varphi_j \in (0, 2\pi)$ where the gain is non-zero. Approximating L_k by $\hat{L}_k$ as in the 2D case, we finally arrive at

$$\mathsf{M}_C(n) \approx \frac{4\pi g^{6/\eta-2}}{n\eta\beta^{3/\eta}}\sum_{k=1}^{n}\gamma\left(\frac{3}{\eta},\frac{\beta\hat{L}_k^\eta}{g^2}\right), \tag{42}$$

and thus obtain $\mathcal{M}(n)$ by finding the minimum of $\mathsf{M}_C(n)$ over all possible antenna orientations

$$\mathcal{M}(n) = \min_{\Theta_i}\mathsf{M}_C(n). \tag{43}$$

This is difficult to calculate analytically, but straightforward numerically, using rotation matrices and a fine grid of Euler angles. The result is shown in Fig. 11 for the range $n \in [2, 30]$ using a cube domain of side $L = 1$, $\beta = 1$, $\lambda = \sqrt{30\pi}/3$ in the top panel and $\lambda = \sqrt{n\pi}/3$ in the lower one. For comparison, all simulations were preformed for path loss values of $\eta = 2, 3,$ and 6. We observe that for $n \leq 13$, there always exist at least one orientation Θ_i such that the pattern does not cover the cubic corner and therefore $\mathcal{M}(n) = 0$, i.e., the multi-directional gain has blind spots. Interestingly, the case of $n = 14$ (corresponding to a polyhedron called a "gyroelongated hexagonal bipyramid" also shown in the inset of the top panel of Fig. 11) covers such corners whilst that of $n = 15$ does not. For larger values of $n \geq 16$, blind spots are always covered, i.e., $\mathcal{M}(n) > 0$. For constant lobe widths characterised by $\lambda = \sqrt{30\pi}/3$, the minimum connectivity mass $\mathcal{M}(n)$ increases with n modulo small fluctuations with better performance at lower path loss. When the lobe widths are scaled by $\lambda = \sqrt{n\pi}/3$, the minimum connectivity mass is approximately constant at $\mathcal{M}(n) \approx 0.15$ for $n \geq 16$ (and $n = 14$) when $\eta = 2$, but decreases steadily for $\eta = 3$, and 6. For comparison, we point out that isotropic radiation would give $\mathsf{M}_C \approx 0.416, 0.427,$ and 0.446 for $\eta = 2, 3,$ and 6 respectively, which is significantly higher than that observed for the multi-directional radiation patterns investigated in Fig. 11. We stress however that Fig. 11 shows only the minimum of $\mathsf{M}_C(n)$ over all possible orientations Θ_i and not the average $\mathsf{M}_C(n)$ which would be a fairer comparison.

Although Fig. 11 is very much domain specific, the above results hint towards an interesting generalization for arbitrarily shaped three dimensional domains. Since at low path loss, increasing the number of lobes and scaling their widths by $\lambda = \sqrt{n\pi}/3$ improves $\mathcal{M}$ while also covering any corner, we propose as an optimal (yet unrealistic) limit a radiation pattern consisting of an infinite number of infinitesimally thin lobes which we call (with a bit of imagination) 'the hedge-hog' pattern; an extreme deformation of the isotropic radiation pattern with $G = 1$ which we showed was optimal for $\eta > d$. Interestingly, the hedge-hog anisotropic pattern is by definition uniform in all orientations and therefore in some sense isotropic.

VIII. Conclusions and Discussion

In this paper, we have investigated the connectivity properties of 3D ad hoc networks with randomly oriented anisotropically radiating nodes. We have shown that for homogeneous systems (i.e. in the absence of boundary effects) the connectivity mass M is a key observable which characterises many important network properties: i) the probability that two randomly selected nodes connect to form a pair, p_2, ii) the network mean degree, μ, iii) the probability of minimum network degree of at least one, $P_{md}(1)$, and finally iv) the probability of obtaining a fully connected network at high node densities, P_{fc}. We therefore focused on the explicit calculation of M for simple but practical antenna gain profiles (e.g. patch, dipole, and end-fire array antennas). Using the analytic expressions obtained, we have identified the ratio of spatial dimension d to path loss η, as a key system parameter. Moreover, we have shown that when the antenna gain is concentrated on a small solid angle ω, the connectivity mass M will scale as $\sim \omega^{2-2d/\eta}$. Significantly, this implies that for $\eta < d$, any directional deformation of the isotropic gain profile will increase M and therefore improve

overall network connectivity. In fact, we find that the more directional the gain, the better connected the network will be. For $\eta > d$ however, all these observations are reversed and isotropic radiation leads to optimal network connectivity. We have validated our results through Monte Carlo computer simulations of the network mean degree and have seen that border effects typically reduce the network mean degree - a feature particularly noticeable for highly directional radiation gains. Extensive numerical simulations have also validated our analytic predictions for $P_{md}(1)$ and the high density expansion of P_{fc} in homogeneous domains. This conclusively confirming our general statement regarding the superiority of directional antennas at low path loss.

Random networks confined within a bounded domain are inhomogeneous systems and therefore boundary effects can have a significant impact on the network connectivity properties. This is because nodes situated near the confinement boundary are likely to be of lower degree than those situated further away. Therefore, the mean network degree is less than expected, particularly for highly directional gains which a) may steer their main beam outside of the domain leading to so called blind spots, and b) at low path loss exponents may have an effective communication range r_0 in their boresight direction which is greater than the typical domain size. We have argued that these two effects have a greater impact for highly directional radiation patterns such as those of an end-fire array. Thus, in contrast to homogeneous systems, directionality in radiation gains is undesirable for networks operating in confined spaces, unless the network can be configured to eliminate the possibility of these eventualities. To this end we have investigated multi-directional radiation patterns as a means to cover both bases (homogeneous and inhomogeneous systems). We emphasize that the results presented in this paper are general and independent of the small-scale fading model used and therefore provide qualitative insight for wireless researchers and practitioners to consider in the future.

Acknowledgements

The authors would like to thank the directors of the Toshiba Telecommunications Research Laboratory for their support.

References

[1] C. D. M. Cordeiro and D. P. Agrawal, *Ad hoc and sensor networks: theory and applications*. World Scientific, 2011.

[2] H. Hartenstein and K. P. Laberteaux, "A tutorial survey on vehicular ad hoc networks," *Communications Magazine, IEEE*, vol. 46, no. 6, pp. 164–171, 2008.

[3] P. Gupta and P. R. Kumar, "Critical power for asymptotic connectivity in wireless networks," in *Stochastic analysis, control, optimization and applications*, pp. 547–566, Springer, 1998.

[4] M. Penrose, *Random geometric graphs*, vol. 5. Oxford University Press Oxford, UK:, 2003.

[5] B. Bollobas and O. Riordan, *Percolation*. Cambridge University Press, 2006.

[6] R. Albert and A.-L. Barabási, "Statistical mechanics of complex networks," *Reviews of modern physics*, vol. 74, no. 1, p. 47, 2002.

[7] R. Rajaraman, "Topology control and routing in ad hoc networks: a survey," *ACM SIGACT News*, vol. 33, no. 2, pp. 60–73, 2002.

[8] S. Bandyopadhyay and E. J. Coyle, "An energy efficient hierarchical clustering algorithm for wireless sensor networks," in *INFOCOM 2003. Twenty-Second Annual Joint Conference of the IEEE Computer and Communications. IEEE Societies*, vol. 3, pp. 1713–1723, IEEE, 2003.

[9] K. Romer and F. Mattern, "The design space of wireless sensor networks," *Wireless Communications, IEEE*, vol. 11, no. 6, pp. 54–61, 2004.

[10] V. Ravelomanana, "Extremal properties of three-dimensional sensor networks with applications," *Mobile Computing, IEEE Transactions on*, vol. 3, no. 3, pp. 246–257, 2004.

[11] M. Younis and K. Akkaya, "Strategies and techniques for node placement in wireless sensor networks: A survey," *Ad Hoc Networks*, vol. 6, no. 4, pp. 621–655, 2008.

[12] G. Mao and B. Anderson, "Towards a better understanding of large-scale network models," *IEEE/ACM Transactions on Networking (TON)*, vol. 20, no. 2, pp. 408–421, 2012.

[13] C. Bettstetter, C. Hartmann, and C. Moser, "How does randomized beamforming improve the connectivity of ad hoc networks?," in *Communications, 2005. ICC 2005. 2005 IEEE International Conference on*, vol. 5, pp. 3380–3385, IEEE, 2005.

[14] H. Koskinen, "Analytical study of connectivity in wireless multihop networks utilizing beamforming," in *Proceedings of the 9th ACM international symposium on Modeling analysis and simulation of wireless and mobile systems*, pp. 212–218, ACM, 2006.

[15] X. Zhou, S. Durrani, and H. M. Jones, "Connectivity analysis of wireless ad hoc networks with beamforming," *Vehicular Technology, IEEE Transactions on*, vol. 58, no. 9, pp. 5247–5257, 2009.

[16] J. Coon and C. Dettmann, "On the connectivity of 2-D random networks with anisotropically radiating nodes," *Communications Letters, IEEE*, vol. 17, no. 2, pp. 321–324, 2013.

[17] H. Xu, H.-N. Dai, and Q. Zhao, "On the connectivity of wireless networks with multiple directional antennas," in *Networks (ICON), 2012 18th IEEE International Conference on*, pp. 155–160, IEEE, 2012.

[18] S. Y. Seidel and T. S. Rappaport, "914 MHz path loss prediction models for indoor wireless communications in multifloored buildings," *Antennas and Propagation, IEEE Transactions on*, vol. 40, no. 2, pp. 207–217, 1992.

[19] R. Ramanathan, "On the performance of ad hoc networks with beamforming antennas," in *Proceedings of the 2nd ACM international symposium on Mobile ad hoc networking & computing*, pp. 95–105, ACM, 2001.

[20] O. Georgiou, C. P. Dettmann, and J. P. Coon, "k-connectivity for confined random networks," *EPL (Europhysics Letters)*, vol. 103, no. 2, p. 28006, 2013.

[21] S. Farrell, V. Cahill, D. Geraghty, I. Humphreys, and P. McDonald, "When TCP breaks: Delay-and disruption-tolerant networking," *Internet Computing, IEEE*, vol. 10, no. 4, pp. 72–78, 2006.

[22] K. Fall and S. Farrell, "DTN: an architectural retrospective," *Selected Areas in Communications, IEEE Journal on*, vol. 26, no. 5, pp. 828–836, 2008.

[23] J. Coon, C. Dettmann, and O. Georgiou, "Full connectivity: corners, edges and faces," *Journal of Statistical Physics*, pp. 1–21, 2012.

[24] G. D. Durgin, T. S. Rappaport, and D. A. De Wolf, "New analytical models and probability density functions for fading in wireless communications," *Communications, IEEE Transactions on*, vol. 50, no. 6, pp. 1005–1015, 2002.

[25] D. Tse and P. Viswanath, *Fundamentals of wireless communication*. Cambridge University Press, 2005.

[26] C. A. Balanis, *Antenna theory: analysis and design*. Wiley-Interscience, 2012.

[27] G. Giorgetti, A. Cidronali, S. K. Gupta, and G. Manes, "Exploiting low-cost directional antennas in 2.4 GHz IEEE 802.15.4 wireless sensor networks," in *Wireless Technologies, 2007 European Conference on*, pp. 217–220, IEEE, 2007.

[28] T. Korakis, G. Jakllari, and L. Tassiulas, "A MAC protocol for full exploitation of directional antennas in ad-hoc wireless networks," in *Proceedings of the 4th ACM international symposium on Mobile ad hoc networking & computing*, pp. 98–107, ACM, 2003.

[29] X. Zhou, S. Durrani, and H. M. Jones, "Analytical study of connectivity in wireless ad hoc networks with random beamforming," *Proc. ICSPCS*, pp. 321–325, 2007.

[30] P. Li, C. Zhang, and Y. Fang, "Asymptotic connectivity in wireless ad hoc networks using directional antennas," *IEEE/ACM Transactions on Networking (TON)*, vol. 17, no. 4, pp. 1106–1117, 2009.

[31] A. Banerjee, R. Agarwal, V. Gauthier, C. K. Yeo, H. Afifi, and F. Lee, "A self-organization framework for wireless ad hoc networks as small worlds," *Vehicular Technology, IEEE Transactions on*, vol. 61, no. 6, pp. 2659–2673, 2012.

[32] R. Ding and R. D. Xiao, "Directional pattern versus omnidirectional pattern of switched beamform antennas for asymptotic connectivity," *Applied Mechanics and Materials*, vol. 235, pp. 147–151, 2012.

[33] "NIST Digital Library of Mathematical Functions." http://dlmf.nist.gov/, Release 1.0.6 of 2013-05-06. Online companion to [40].
[34] Z. Khalid and S. Durrani, "Connectivity of three dimensional wireless sensor networks using geometrical probability," in *Communications Theory Workshop (AusCTW), 2013 Australian*, pp. 47–51, IEEE, 2013.
[35] F. Fabbri, C. Buratti, and R. Verdone, "A multi-sink multi-hop wireless sensor network over a square region: Connectivity and energy consumption issues," in *GLOBECOM Workshops, 2008 IEEE*, pp. 1–6, IEEE, 2008.
[36] P. Fan, G. Li, K. Cai, and K. Letaief, "On the geometrical characteristic of wireless ad-hoc networks and its application in network performance analysis," *Wireless Communications, IEEE Transactions on*, vol. 6, no. 4, pp. 1256–1265, 2007.
[37] J. Guo, S. Durrani, and X. Zhou, "Outage probability in arbitrarily-shaped finite wireless networks," *Communications, IEEE Transactions on*, vol. PP, no. 99, pp. 1–14, 2014.
[38] D. J. Wales and S. Ulker, "Structure and dynamics of spherical crystals characterized for the thomson problem," *Physical Review B*, vol. 74, no. 21, p. 212101, 2006.
[39] "Global Minima for the Thomson Problem." http://www-wales.ch.cam.ac.uk/ wales/CCD/Thomson/table.html, Dated 15-12-2006. Online companion to [38].
[40] F. W. J. Olver, D. W. Lozier, R. F. Boisvert, and C. W. Clark, eds., *NIST Handbook of Mathematical Functions*. New York, NY: Cambridge University Press, 2010.